Chinese Journal of Physics 69 (2021) 134–142

Contents lists available at ScienceDirect

Chinese Journal of Physics

journal homepage: www.sciencedirect.com/journal/chinese-journal-of-physics

Solution combustion synthesis of $NaFePO_4$ and its electrochemical performance

S.N. Yadav [a,b], S.J. Rajoba [a,c], R.S. Kalubarme [d], V.G. Parale [e], L.D. Jadhav [a,*]

[a] Electrochemical Energy Materials Laboratory, Department of Physics, Rajaram College, Kolhapur, 416 004, India
[b] School of Nanoscience and Technology, Shivaji University, Kolhapur 416004, India
[c] Department of Physics, Tuljaram Chaturchand College, Baramati 413 102, India
[d] Centre for Materials for Electronics Technology, Thrissur, 680581, India
[e] Department of Materials Science and Engineering, Yonsei University, 50 Yonsei-ro, Seodaemun-gu, Seoul 03722, South Korea

ARTICLE INFO

Keywords:
Cathode material
maricite $NaFePO_4$
combustion
sodium-ion battery

ABSTRACT

In the current research work, submicron size single-phase $NaFePO_4$ (NFP) nanoparticles are successfully synthesized using the solution combustion method. The calcination of as synthesized NFP powder is done at 700 °C for 5h in the air atmosphere and it shows the maricite phase crystallized into an orthorhombic structure with a surface area of 9.29 m^2/g. The intermolecular vibrations of the $(PO_4)^{3-}$ group are identified in the FTIR spectra. The XPS spectra of NFP confirms the presence of Fe and P in +2 and +5 oxidation states, respectively. The coin cell assembled using calcined NFP powder shows a pair of redox peaks at 2.42 and 2.69 V vs. Na/Na^+ owing to Na-ion insertion and extraction. NFP material delivers a specific capacity of 28 mAh/g at 0.1 C with 92% capacity retention after 35 cycles.

1. Introduction

Lithium-ion batteries (LIBs) are outstanding in terms of performance, delivering high capacity with longer cycle life and have been commonly used in recent portable electronic devices like cell phones, cameras, and laptops [1] besides their huge potential in electric vehicle and power grid applications [2]. Lithium iron phosphate ($LiFePO_4$) is one of the gifted cathode materials in the LIBs as it demonstrates the remarkable theoretical capacity and cycle stability [3,4,5]. The state-of-art anode material is either metallic Li or graphite but both suffer from certain issues that have been successfully addressed in the newly developed anode materials such as transition metal oxides, vanadium based oxides, etc [6]. Despite being environmentally benign, the high cost and shortage of lithium resources are the major problems with large-scale energy storage applications [7]. Meanwhile, sodium-ion batteries (SIBs) have shown increasing interest as one of the most capable next-generation power sources owing to its comparable theoretical capacity and energy storage density to that of Li counterpart [8]. An enormous availability and low cost of sodium make the SIBs a better option for LIBs. Moreover, the rocking-chair mechanism is analogous to the same observed in the LIBs [9], which made understanding of the phenomenon quite simpler. Particularly, the cathode materials performing intercalation chemistry in SIBs have relatively high voltage and good thermal stability. The cathode materials include layered and tunnel type transition metal oxides ($NaVoO_2$, $NaFeO_2$, and $NaMnO_2$) [10,11,12], phosphate-based polyanions ($Na_3V_2(PO_4)_2F_3$, $Na_4Fe_3(PO_4)_2(P_2O_7)$ [13], sulphates ($Na_2Fe_3(SO_4)_3$) [14], pyrophosphate ($Na_2FeP_2O_7$) [15], as well as prussian blue analogs ($Na_{0.61}Fe[Fe(CN)_6]_{0.94}$) [16,17], and polymers (polyamides) [18]. Among them,

* Corresponding author.
E-mail address: ldjadhav.phy@gmail.com (L.D. Jadhav).

https://doi.org/10.1016/j.cjph.2020.11.020
Received 3 September 2020; Received in revised form 7 November 2020; Accepted 27 November 2020
Available online 8 December 2020

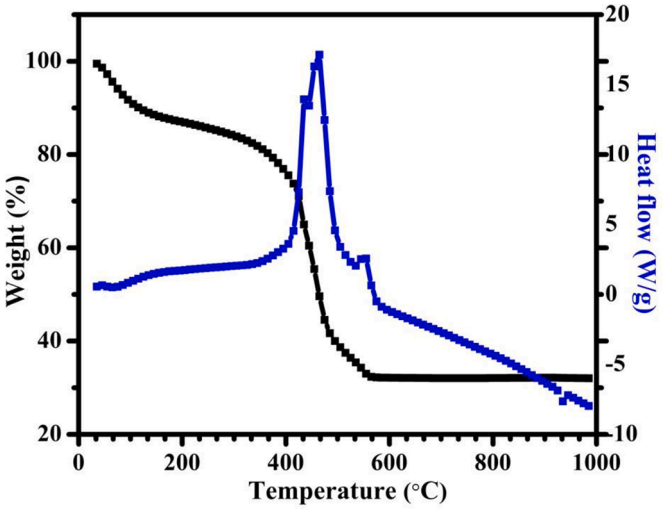

Fig. 1. TG-DTA of as prepared $NaFePO_4$ powder

phosphate-based polyanions have attracted tremendous attention because of high voltage and good thermal stability [19]. Specifically, sodium iron phosphate ($NaFePO_4$) having low cost and high theoretical capacity (~154 mAh/g) can be considered as a cathode material [20,21].

However, $NaFePO_4$ exists in two phases namely maricite and olivine. The latter being thermodynamically unstable [22] is often obtained by replacing Li ions in $LiFePO_4$ with Na ions, shows good electrochemical performance [23]. On the contrary, the thermodynamically stable maricite phase possesing relatively closed packed structures is reported to be electrochemically inactive because of the non-availability of Na ion diffusion paths [24]. However, few papers reported electrochemical performance of $NaFePO_4$, comparatively lower than its olivine phase. The specific capacities of $NaFePO_4$ synthesized by hydrothermal [25] and modified Pechini approach [26] were 20 mAh/g at 0.048 mA/g and 25 mAh/g, respectively. Kapaev *et al.* [27] showed that the capacity of m-$NaFePO_4$@carbon composite could be increased from 15-27 mAh/g to nearly 150 mAh/g after applying planetary ball milling.

The present paper reports on the synthesis of $NaFePO_4$ by solution combustion approach. It is one of the attractive and simple techniques to synthesize nanoparticles [28–30]. It involves a self-sustained reaction between an oxidizer and fuel promoting the easy synthesis of a variety of metal nanoparticles, complex oxides, alloys, and composites in the form of nanoscale powders [31]. Also, the paper reports on the physical properties of synthesized $NaFePO_4$.

2. Experimental

The synthesis of $NaFePO_4$ (NFP) nanoparticles as a cathode material was carried out by using solution combustion synthesis (SCS) method. The oxidants used were the nitrates of iron ($Fe(NO_3)_3.9H_2O$: 3.04 g) and sodium ($NaNO_3$: 3.06 g), and ammonium dihydrogen phosphate ($NH_4H_2PO_4$: 5.3 g). The fuel was citric acid ($C_6H_8O_7$) and all the chemicals used were of purchased from Alfa Aesar . The stoichiometric amounts of oxidants and fuel were dissolved in the minimum quantity of double distilled water. The solution was then allowed to stir to make a homogenous mixture and was simultaneously heated to remove excess water. The pH of the precursor solution was regulated by using ammonia. The stirring and heating was continued until the gel formation and this gel was allowed to combust in a preheated furnace. The obtained combustion product was black-grey colored foam which was ground in an agate mortar to get the homogenous fine grained powder. This as synthesized powder was subjected to heat treatment in the furnace in the air atmosphere at 700 °C for 5h.

2.1. Characterization of $NaFePO_4$

Thermogravimetric (TG) and differential thermal analysis (DTA) profiles of as synthesized $NaFePO_4$ powder were obtained using the Perkin Elmer instrument (model SDT-2960), and measured from room temperature to 1000°C with a variable scan rates in different atmospheres. The crystalline properties of as-prepared and calcined $NaFePO_4$ powder were determined by using an X-ray diffractometer (PHILIPS PW-3710) with CuK_α as a radiation source. The morphology of the particles was analyzed by scanning electron microscopy (JEOL JSM 6360 Japan). The chemical functional groups present in the sample were determined using Fourier transform infra-red (FTIR) spectroscopy, N_2 adsorption-desorption isotherms were measured with the help of Quantachrome Instruments v10.0 and the specific surface area was calculated using Brunauer-Emmett-Teller (BET) method. X-ray photoelectron spectroscopy (XPS) was carried out with the help of K-alpha (Thermo VG instrument with Al K_α line of 1486.6 eV) spectrometer to determine the surface electronic states present in the calcined $NaFePO_4$ powder. The obtained XPS data was calibrated using the C 1s peak of adventitious aliphatic carbon, and finally a Shirley-type background correction was applied.

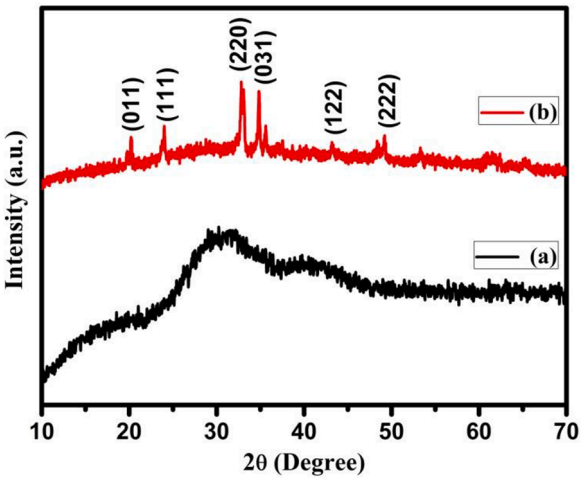

Fig. 2. XRD patterns of (a) as prepared powder, and (b) powder calcined at 700 °C for 5 h

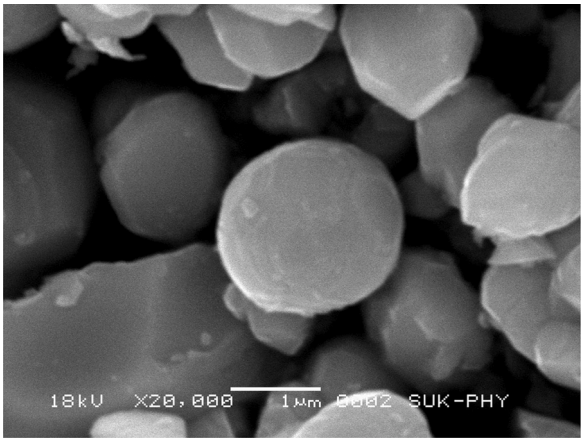

Fig. 3. SEM image of NFP powder calcined at 700 °C

2.2. Electrode fabrication

To fabricate the working electrode, 70% $NaFePO_4$ powder was mixed with 20% carbon black and 10% polyvinylidene fluoride (PVDF) binder dissolved in N-methyl-2- pyrrolidone (NMP). The prepared slurry was coated on an aluminum foil by a doctor-blade method. The dried film was punched into the shape of a disc of 16 mm diameter. The coin cells were assembled with sodium metal foil as a reference electrode and celgard 2400 membrane as a separator. The $NaPF_6$ in ethylene carbonate (EC), diethyl carbonate (DEC) and dimethyl carbonate (DMC) in 1:1:1 ratio was used as an electrolyte. The assembling was done in the glove box filled with argon. The cyclic voltammetry, galvanostatic charge-discharge, and electrochemical impedance spectroscopy (EIS) measurements were carried at various scan rates by using the Bio-Logic instrument (BCS-810, France).

3. Results and discussion

TG-DTA plot of as-prepared $NaFePO_4$ powder in the air atmosphere is shown in Fig. 1. An initial weight loss was observed up to 150 °C and it was due to the removal of loosely adsorbed water. Further reduction in the weight observed up to 550 °C along with strong exothermic peaks at 440 °C and 488 °C can be assigned to the oxidation of remaining nitrates, the formation of secondary Na based phases, or transformation of $NaFePO_4$ from olivine to maricite phase [32]. The weight loss is not observed above 600 °C, which affirms no further structural or phase change in the material. Hence the calcination temperature of $NaFePO_4$ powder was fixed as 700 °C.

The XRD pattern of as-prepared NFP powder is as shown in Fig. 2 (a). The as-prepared powder was confirmed as highly amorphous, as no peaks in the XRD pattern are observed. To enhance the crystallinity of the material, the prepared powder was calcined at 700 °C for 5h in the air atmosphere, and its XRD pattern is presented in the Fig. 2 (b). Surprisingly, the powder is crystallized into $NaFePO_4$ without the formation of any intermediate/secondary phases, unlike earlier studies where heat treatment in the air atmosphere had led

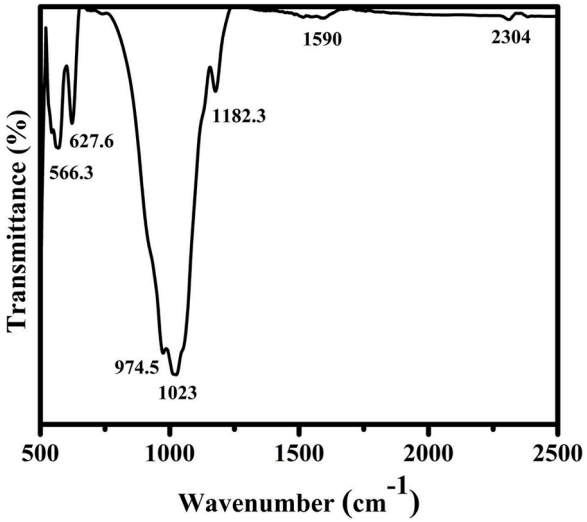

Fig. 4. FTIR spectrum of NFP powder calcined at 700 °C

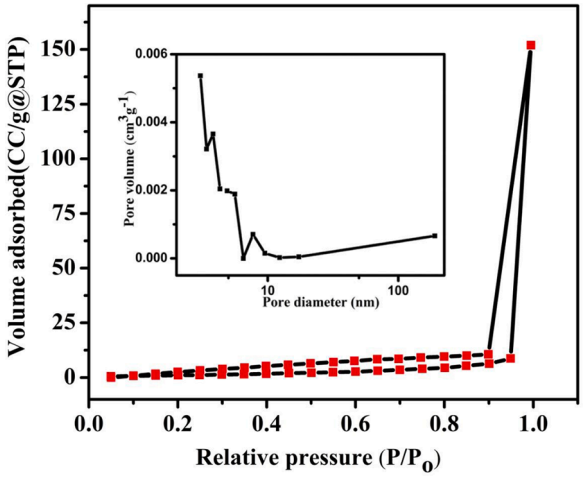

Fig. 5. The nitrogen adsorption/desorption isotherms of NFP powder. The inset shows pore size distribution

to the formation of secondary phases [28]. The reducing atmosphere created by the fuel (citric acid) during combustion prevented the formation of the intermediate/secondary phases. The observed XRD pattern is compared with the standard data for the maricite phase (JCPDS:29-1216) [33]. The structure of the material is orthorhombic with lattice constants $a = 7.0$ Å, $b = 8.92$ Å, and $c = 5.02$ Å. The Debye Scherrer equation mentioned in equation (1) was used to determine the crystallite size.

$$D = \frac{K\lambda}{\beta\cos\theta} \tag{1}$$

The average crystallite size is 32 nm.

Fig. 3 shows an SEM image of NFP powder calcined at 700 °C. This shows nearly round-shaped grains. The edges of some of the grains have fine cuts at the boundaries. The average size of the grains is 1.45 μm.

The FTIR spectrum of $NaFePO_4$ powder is provided in the Fig. 4. The intermolecular vibrations of the PO_4 group are observed in the FTIR spectrum. The bands observed in the wavenumber region 900 to 1150 cm^{-1} are due to symmetric (ν_1) and asymmetric (ν_3) stretching modes whereas bands in the region 500 to 650 cm^{-1} are due to the symmetric (ν_2) and asymmetric (ν_4) bending modes [34]. Specifically, FTIR spectrum reveals well defined characteristic stretching and bending vibrations of the phosphate anion $(PO_4)^{3-}$. The stretching modes are observed at 974.5 cm^{-1} (ν_1) and 1023 cm^{-1} (ν_3), while the bending modes are observed at 566.3 cm^{-1} (ν_4) and 627.6 cm^{-1} (ν_2) [20,35]. Moreover, the weak bands at 1182 and 1590 cm^{-1} are ascribed to the stretching vibrations of C-O bond and another weak band at 2304 cm^{-1} is assigned to C-H stretching vibration. This carbon content originates from the consumption of citric acid used as fuel for the synthesis of NFP [36].

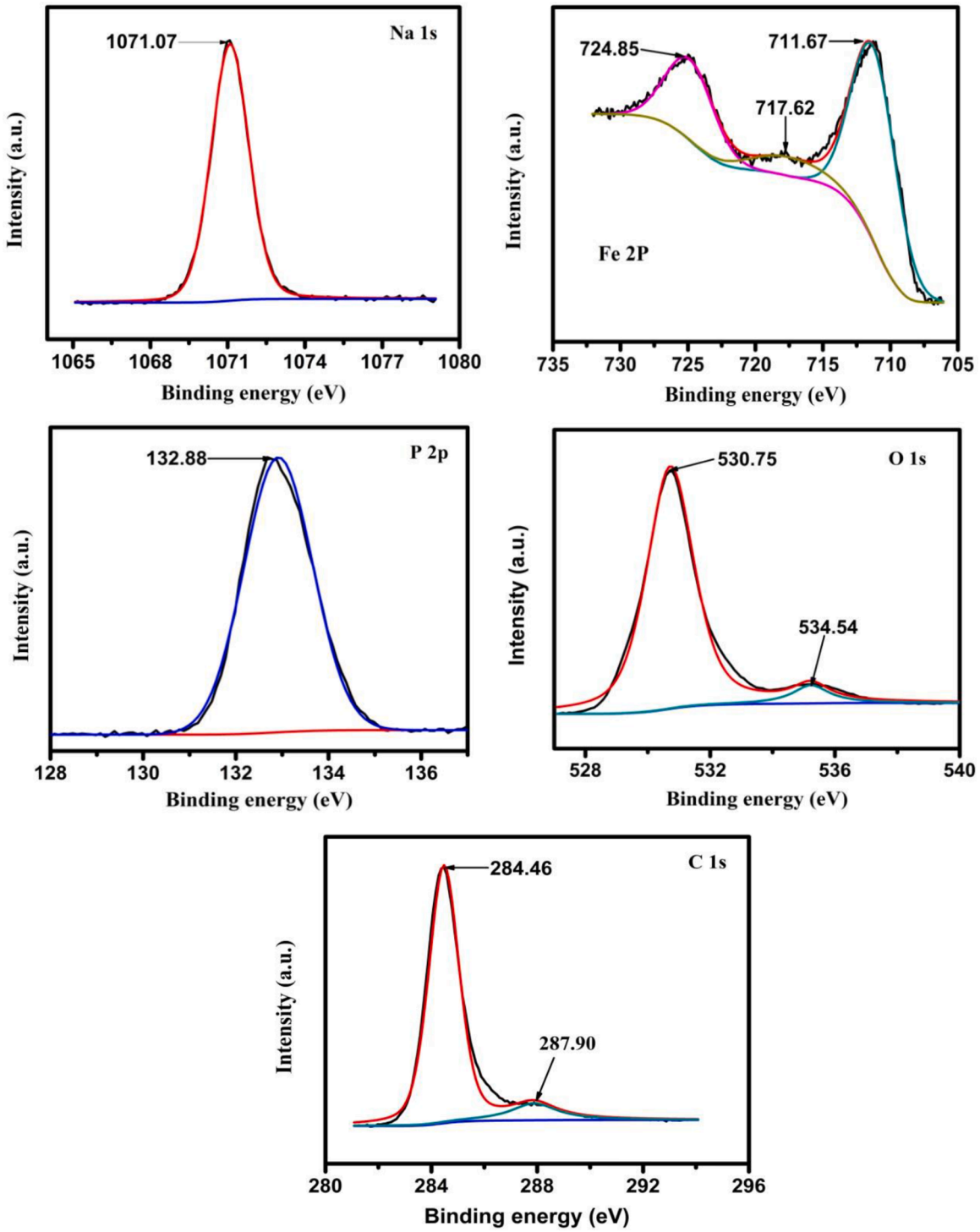

Fig. 6. XPS spectrum of NFP powder calcined at 700 °C

The N_2 adsorption-desorption isotherms and pore size distribution of calcined NFP powder are shown in Fig. 5. Brunauer-Emmett-Teller (BET) method was used to estimate surface area. The calculated surface area is 9.29 m^2/g, which is quite high to improve the electronic conductivity while average pore radius is 5.37 nm (the inset of Fig 5), representing a mesoporous structure favorable for diffusion enabled processes during intercalation and deintercalation.

XPS spectrum was recorded for NFP powder calcined in air at 700 °C. The wide scan spectra for Na 1s, Fe 2p, P 2p, O 1s and C 1s are

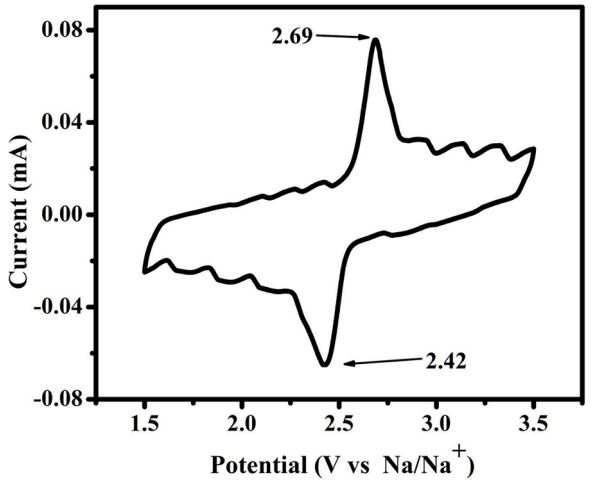

Fig. 7. Cyclic voltammetry of NFP electrode at a scan rate of 0.1mV/s

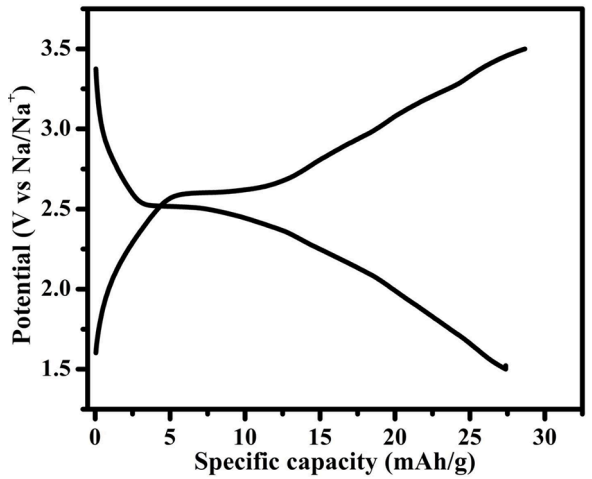

Fig. 8. Charge-discharge profile of NFP electrode at 0.1 C

Table 1
Comparison of specific capacities of $NaFePO_4$ with the values reported in the literature

Sr. No.	Structure	Method	Specific Capacity ($mAhg^{-1}$)	Surface area (m^2/g)	C-rate	Reference
1.	M-$NaFePO_4$	Solution combustion synthesis	28	9.29	0.1	Present work
2.	Maricite-$NaFePO_4$	Solid state route	20	5.3	0.1	25
3.	Maricite $NaFePO_4$/C	Two-step solid-state route	48.8	-	0.05	33
4.	Maricite -$NaFePO_4$	Pechini process	25	-	0.1	26
5.	M-$NaFePO_4$@ carbon	Modified Pechini process	27	-	0.1	27

presented in Fig. 6. The Na 1s peak is observed at binding energy 1071.07 eV. As shown in the Fig 6, the Fe 2p spectrum splits into two levels due to spin-orbit coupling. These Fe $2p_{3/2}$ and Fe $2p_{1/2}$ levels are observed at binding energies 711.67 and 724.85 eV, respectively. In addition, it shows satellite peak at 717.62 eV corresponding to Fe $2p_{3/2}$ and originated due to partially filled d-orbitals of Fe. The binding energy difference (spin-orbit splitting) between Fe $2p_{3/2}$ and Fe $2p_{1/2}$ levels is 13.18 eV. This identifies Fe in +2 state. The P in phosphate anion ($(PO_4)^{3-}$) is in +5 state with binding energy 132.88 eV. The O 1s spectrum shows two peaks at 530.75 and 534.54 eV, the former intense one is due to O^{2-} in the crystal lattice while the later can be assigned to adsorbed oxygen species and oxygen-containing groups attached to the carbon. The C1s peak at binding energy of 284.46 eV indicates the presence of graphitic carbon in addition to C=O contribution at 287.9 eV.

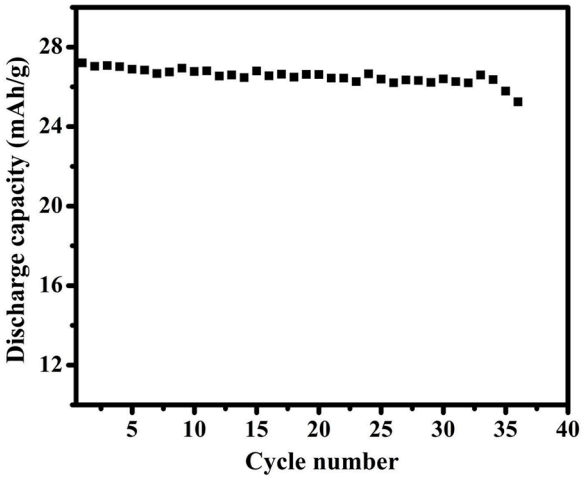

Fig. 9. Cycling stability of NFP electrode at 0.1 C.

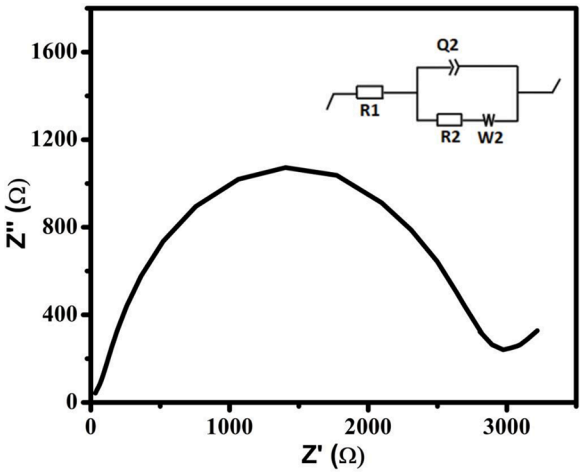

Fig. 10. Electrochemical impedance spectroscopy (EIS) of NFP

4. Electrochemical measurements

The cyclic voltammetry (CV) curve of NFP electrode in the voltage range 1.5 to 3.5 V at a scan rate of 0.1mV/s is shown in Fig. 7. The cathodic and anodic peaks are observed at 2.42 and 2.69 V (vs. Na/Na^{+}), respectively representing redox process due to the two-step Na-ion insertion and extraction mechanism. Besides, a few more peaks due to the presence of electroactive impurities are observed but no impurities are evident in the XRD pattern. The CV curve also shows some capacitive contribution.

The charge-discharge profile of NFP electrode at 0.1 C is shown in Fig. 8. The NFP delivers a specific capacity of 28 mAh/g at 0.1 C. Such a small specific capacity has also been reported by Ling Zhao et al [33] and others as tabulated in the Table 1. It has been reported that the specific capacity of material could be improved by increasing defect concentration or by decreasing the particle size [27].

The cyclic stability of NFP electrode at 0.1 C is shown in Fig. 9. The capacity retention is observed to be 92% after 35 cycles. The electrochemical impedance spectroscopy (EIS) of NFP is provided in Fig. 10. It comprises a depressed semicircle at a higher frequency and a tail at a lower frequency. The data were fitted using BT-Lab V1.64 (Biologic-810) software and electrochemical processes taking place can be represented by equivalent circuit $R_1 + Q_2/ (R_2 + W_2)$ (inset of Fig. 10), where R_1, R_2, and W_2 respectively represents ohmic, charge transfer, and Warburg resistance and Q_2 represents capacitance. The fitted values are R_1=41.57 Ω, R_2=2814 Ω, and Q_2=3.974 × 10^{-6} F. Further the slope of the straight line indicates low Na ion diffusion during the electrochemical reaction [37]. EIS reveals that the high value of charge transfer resistance of the cell is restricting the discharge capacity of NFP.

5. Conclusions

In summary, the maricite-$NaFePO_4$ has been successfully synthesized using low-cost, environmentally friendly, and potentially

scalable solution combustion method. The crystallite size of the prepared powder is 32 nm. A well defined characteristic stretching and bending vibrations of $(PO_4)^{3-}$ are observed in the region 900 to 1150 cm^{-1} and 500 to 650 cm^{-1}, respectively. The binding energy difference between Fe $2p_{3/2}$ and Fe $2p_{1/2}$ levels is 13.18 eV validating the presence of bivalence Fe. Although the majority of the research reports claimed that the maricite phase is electrochemically inactive, we are among the few reporting specific capacity of 28 mAh/g at 0.1C and it is assigned to the presence of mesoporous particles. Further work is in progress to comprehend the underlying charge transfer mechanism to minimize the charge transfer resistance and enhance the specific capacity.

Declaration of Competing Interest

The authors declare that they have no known competing financial interests or personal relationships that could have appeared to influence the work reported in this paper.

Acknowledgment

One of the authors S. N. Yadav acknowledges the financial support by the Government of Maharashtra's Chhatrapati Shahu Maharaj Research Training and Human Development Institute (SARTHI), Pune.

References

[1] S.J. Rajoba, L.D. Jadhav, R.S. Kalubarme, P.S. Patil, S. Varma, B.N. Wani, Electrochemical performance of LiFePO4/GO composite for Li-ion batteries, Ceram. Int 44 (2018) 6886–6893, https://doi.org/10.1016/j.ceramint.2018.01.114.
[2] K. Jayaramulu, D.P. Dubal, A. Schneemann, V. Ranc, C. Perez-Reyes, J. Stráská, Š. Kment, M. Otyepka, R.A. Fischer, R. Zbořil, Shape-assisted 2D MOF/graphene derived hybrids as exceptional lithium-ion battery electrodes, Adv. Funct. Mater 29 (2019) 1–11, https://doi.org/10.1002/adfm.201902539.
[3] S.J. Rajoba, L.D. Jadhav, R.S. Kalubarme, S.N. Yadav, Influence of synthesis parameters on the physicochemical and electrochemical properties of LiFePO4 for Li-ion battery, J. Alloys Compd 774 (2019) 841–847, https://doi.org/10.1016/j.jallcom.2018.09.325.
[4] B. Lung-Hao Hu, F.Y. Wu, C. Te Lin, A.N. Khlobystov, L.J. Li, Graphene-modified LiFePO4 cathode for lithium ion battery beyond theoretical capacity, Nat. Commun 4 (2013) 1–7, https://doi.org/10.1038/ncomms2705.
[5] R. Kashi, M. Khosravi, M. Mollazadeh, Effect of carbon precursor on electrochemical performance of LiFePO4-C nano composite synthesized by ultrasonic spray pyrolysis as cathode active material for Li ion battery, Mater. Chem. Phys 203 (2018) 319–332, https://doi.org/10.1016/j.matchemphys.2017.10.021.
[6] D. Dubal, D. Patil, S. Patil, P. Gomez-romero, BiVO4 Fern Architectures, A competitive anode for Li-ion batteries, ChemSusChem 10 (2017) 4163–4169, https://doi.org/10.1002/cssc.201701483.
[7] J. Kim, D.H. Seo, H. Kim, I. Park, J.K. Yoo, S.K. Jung, Y.U. Park, W.A. Goddard, K. Kang, Unexpected discovery of low-cost maricite NaFePO4 as a high-performance electrode for Na-ion batteries, Energy Environ. Sci 8 (2015) 540–545, https://doi.org/10.1039/c4ee03215b.
[8] M. Chen, Y. Zhang, G. Xing, Y. Tang, Building high power density of sodium-ion batteries: importance of multidimensional diffusion pathways in cathode materials, Front. Chem 8 (2020) 1–7, https://doi.org/10.3389/fchem.2020.00152.
[9] E. Wang, M. Chen, X. Liu, Y. Liu, H. Guo, Z. Wu, W. Xiang, B. Zhong, X. Guo, S. Chou, S.X. Dou, Organic cross-linker enabling a 3D porous skeleton–supported Na3V2(PO4)3/Carbon composite for high power sodium-ion battery cathode, Small Methods 3 (2019) 1–10, https://doi.org/10.1002/smtd.201800169.
[10] D. Hamani, M. Ati, J.M. Tarascon, P. Rozier, NaxVO2 as possible electrode for Na-ion batteries, Electrochem. Commun 13 (2011) 938–941, https://doi.org/10.1016/j.elecom.2011.06.005.
[11] N. Yabuuchi, H. Yoshida, S. Komaba, Crystal structures and electrode performance of alpha-NaFeO2 for rechargeable sodium batteries, Electrochemistry 80 (2012) 716–719, https://doi.org/10.5796/electrochemistry.80.716.
[12] X. Ma, H. Chen, G. Ceder, Electrochemical properties of monoclinic NaMnO2, J. Electrochem. Soc. 158 (2011) A1307–A1312, https://doi.org/10.1149/2.035112jes.
[13] A. Mauger, C.M. Julien, State-of-the-art electrode materials for sodium-ion batteries, Materials (Basel) 13 (2020) 3453, https://doi.org/10.3390/MA13163453.
[14] P. Barpanda, G. Oyama, S.I. Nishimura, S.C. Chung, A. Yamada, A 3.8-V earth-abundant sodium battery electrode, Nat. Commun. 5 (2014) 4358, https://doi.org/10.1038/ncomms5358.
[15] P. Barpanda, T. Ye, S.I. Nishimura, S.C. Chung, Y. Yamada, M. Okubo, H. Zhou, A. Yamada, Sodium iron pyrophosphate: a novel 3.0 v iron-based cathode for sodium-ion batteries, Electrochem, Commun 24 (2012) 116–119, https://doi.org/10.1016/j.elecom.2012.08.028.
[16] Y. You, X. Yu, Y. Yin, K.W. Nam, Y.G. Guo, Sodium iron hexacyanoferrate with high Na content as a Na-rich cathode material for Na-ion batteries, Nano Res 8 (2014) 117–128, https://doi.org/10.1007/s12274-014-0588-7.
[17] X. Wu, C. Wu, C. Wei, L. Hu, J. Qian, Y. Cao, X. Ai, J. Wang, H. Yang, Highly crystallized Na2CoFe(CN)6 with suppressed lattice defects as superior cathode material for sodium-ion batteries, ACS Appl. Mater. Interfaces 8 (2016) 5393–5399, https://doi.org/10.1021/acsami.5b12620.
[18] Q. Zhao, A.K. Whittaker, X.S. Zhao, Polymer electrode materials for sodium-ion batteries, Materials (Basel) 11 (2018) 2567, https://doi.org/10.3390/ma11122567.
[19] C. Heubner, S. Heiden, M. Schneider, A. Michaelis, In-situ preparation and electrochemical characterization of submicron sized NaFePO4 cathode material for sodium-ion batteries, Electrochim. Acta 233 (2017) 78–84, https://doi.org/10.1016/j.electacta.2017.02.107.
[20] X. Ma, J. Xia, X. Wu, Z. Pan, P.K. Shen, Remarkable enhancement in the electrochemical activity of maricite NaFePO4 on high-surface-area carbon cloth for sodium-ion batteries, Carbon N. Y 146 (2019) 78–87, https://doi.org/10.1016/j.carbon.2019.02.004.
[21] N. Wongittharom, T.C. Lee, C.H. Wang, Y.C. Wang, J.K. Chang, Electrochemical performance of Na/NaFePO4 sodium-ion batteries with ionic liquid electrolytes, J. Mater. Chem. A. 2 (2014) 5655–5661, https://doi.org/10.1039/c3ta15273a.
[22] M.Y. Zheng, Z.Y. Bai, Y.W. He, S. Wu, Y. Yang, Z.Z. Zhu, Anionic redox processes in maricite- and triphylite-NaFePO4 of sodium-ion batteries, ACS Omega 5 (2020) 5192–5201, https://doi.org/10.1021/acsomega.9b04213.
[23] S. Jeong, B.H. Kim, Y.D. Park, C.Y. Lee, J. Mun, A. Tron, Artificially coated NaFePO4 for aqueous rechargeable sodium-ion batteries, J. Alloys Compd 784 (2019) 720–726, https://doi.org/10.1016/j.jallcom.2019.01.046.
[24] H.H. Kim, I.H. Yu, H.S. Kim, H.J. Koo, M.H. Whangbo, On why the two polymorphs of NaFePO4 exhibit widely different magnetic structures: density functional analysis, Inorg. Chem 54 (2015) 4966–4971, https://doi.org/10.1021/acs.inorgchem.5b00577.
[25] P.P. Prosini, C. Cento, A. Masci, M. Carewska, Sodium extraction from sodium iron phosphate with a Maricite structure, Solid State Ionics 263 (2014) 1–8, https://doi.org/10.1016/j.ssi.2014.04.019.
[26] A. Sun, F.R. Beck, D. Haynes, J.A. Poston, S.R. Narayanan, P.N. Kumta, A. Manivannan, Synthesis, characterization, and electrochemical studies of chemically synthesized NaFePO4, Mater. Sci. Eng. B Solid-State Mater. Adv. Technol 177 (2012) 1729–1733, https://doi.org/10.1016/j.mseb.2012.08.004.
[27] R.R. Kapaev, A.A. Chekannikov, S.A. Novikova, T.L. Kulova, A.M. Skundin, A.B. Yaroslavtsev, Activation of NaFePO4 with maricite structure for application as a cathode material in sodium-ion batteries, Mendeleev Commun 27 (2017) 263–264, https://doi.org/10.1016/j.mencom.2017.05.015.
[28] S.J. Rajoba, L.D. Jadhav, P.S. Patil, D.K. Tyagi, S. Varma, B.N. Wani, Enhancement of Electrical Conductivity of LiFePO4 by controlled solution combustion synthesis, J. Electron. Mater. 46 (2017) 1683–1691, https://doi.org/10.1007/s11664-016-5212-z.

[29] S.T. Jadhav, S.U. Dubal, A.P. Jamale, S.P. Patil, C.H. Bhosale, V.R. Puri, L.D. Jadhav, Structural, morphological and electrical studies of BaCe0.8Y0.2O3-δ synthesized by solution combustion method, Ionics (Kiel). 21 (2015) 1295–1300. 10.1007/s11581-014-1304-z.
[30] A.U. Chavan, L.D. Jadhav, A.P. Jamale, S.P. Patil, C.H. Bhosale, S.R. Bharadwaj, P.S. Patil, Effect of variation of NiO on properties of NiO/GDC (gadolinium doped ceria) nano-composites, Ceram. Int 38 (2012) 3191–3196, https://doi.org/10.1016/j.ceramint.2011.12.023.
[31] T. Mimani, K.C. Patil, Solution combustion synthesis of nanoscale oxides and their composites, 4 (2001) 134–137.
[32] P. Moreau, D. Guyomard, J. Gaubicher, F. Boucher, Structure and stability of sodium intercalated phases in olivine FePO4, Chem. Mater 22 (2010) 4126–4128. https://pubs.acs.org/doi/10.1021/cm101377h.
[33] L. Zhao, D. Zhou, W. Huang, X. Kang, Q. Shi, Z. Deng, X. Yan, Y. Yu, Electrochemical performances of maricite NaFePO4/C as cathode material for sodium-ion and lithium-ion batteries, Int. J. Electrochem. Sci 12 (2017) 3153–3165, https://doi.org/10.20964/2017.04.35.
[34] N.V. Kosova, A.B. Slobodyuk, O.A. Podgornova, Comparative structural analysis of LiMPO4 and Li2MPO4F (M = Mn, Fe, Co, Ni) according to XRD, IR, and NMR spectroscopy data, J, Struct. Chem. 57 (2016) 345–353, https://doi.org/10.1134/S0022476616020153.
[35] C. Murugesan, S. Lochab, B. Senthilkumar, P. Barpanda, Earth-abundant alkali iron phosphates (AFePO4) as efficient electrocatalysts for the oxygen reduction reaction in alkaline solution, ChemCatChem 10 (2018) 1122–1127, https://doi.org/10.1002/cctc.201701423.
[36] D. Wyrzykowski, E. Hebanowska, G. Nowak-Wiczk, M. Makowski, L. Chmurzyński, Thermal behaviour of citric acid and isomeric aconitic acids, J. Therm. Anal. Calorim. 104 (2011) 731–735, https://doi.org/10.1007/s10973-010-1015-2.
[37] Y. Zhu, Y. Xu, Y. Liu, C. Luo, C. Wang, Comparison of electrochemical performances of olivine NaFePO4 in sodium-ion batteries and olivine LiFePO4 in lithium-ion batteries, Nanoscale 5 (2013) 780–787, https://doi.org/10.1039/c2nr32758a.